Icarus 139, 81–92 (1999)
Article ID icar.1999.6087, available online at http://www.idealibrary.com on IDEAL®

Corona Classification by Evolutionary Stage

John E. DeLaughter

Chevron Petroleum Technology Company, La Habra, California 90633

and

Donna M. Jurdy

Department of Geological Sciences, Northwestern University, Evanston, Illinois 60208-2150
E-mail: donna@earth.nwu.edu

Received February 26, 1998; revised September 2, 1998

The formation of coronae, abundant volcano-tectonic features on the surface of Venus, has been modeled as the interaction of mantle diapirs with the lithosphere. However, the applicability of this model to features of widely different sizes may not be evident from SAR images due to the lack of a common scale. We use the radius as a scaling parameter for both the distance from the center and relief, obviating this problem, and mapping the effects from coronae of different radii onto a single scale. Normalizing profiles for 394 features, we find many features classified by E. R. Stoffan *et al.* (1992, *J. Geophys. Res.* 97, 13,347–13,378) as different types have very similar profiles and relief. Coronae distribute into three shapes (domal, circular, calderic); two shapes not related to coronae (radial and volcanic) remain. Variation between corona shapes is gradational and mirrors the evolution of diapirs from initial domal upwellings to calderas. We test the implied age progression using impact crater populations within three corona radii. Despite the inherent uncertainties of this method, crater statistics for a size-restricted (275–325 km) corona set suggest an age progression from domal through circular to calderic. The calderic coronae have an associated impact crater population very similar to the global mean, though with slightly too few tectonized craters, implying that they approximate the average surface age and are no longer active. The circular coronae have a low impact crater density and a slightly elevated proportion of tectonized craters and thus are currently active. The domal coronae have fewer than the expected number of impact craters, of which more are tectonized than expected, suggesting that surface modification has begun.

Key Words: Venus; coronae; craters.

1. INTRODUCTION

The surface of Venus has a mean age of ~288 Myr inferred from the number of impact craters observed (Strom *et al.* 1994) and lacks apparent plate tectonic features. Several authors (e.g., Schaber *et al.* 1992, Strom *et al.* 1994, Herrick 1994) have suggested that Venus underwent a major resurfacing event at some time in the past, based on the distribution of impact craters and the proportion of pristine craters. Even though they argue that less than 6% of Venus' surface has been volcanically resurfaced in the past 288 myr, Strom *et al.* (1994) have found that there are twice as many heavily fractured impact craters and 1.4 times more lava-embayed craters as expected within a region bounded by 30°N and 30°S and 60° and 300°E. This area contains the Beta–Atla–Themis ("BAT") region which may be a region of major upwelling (Crumpler *et al.* 1993); others (Squyres *et al.* 1992, Stofan *et al.* 1992, Stefanick and Jurdy 1996, Nagasawa *et al.* 1997) observed that the coronae are clustered in this region.

Alternatively, from the relation of crater density to radar cross section and modified craters, Phillips *et al.* (1992) have argued that Venus may be in a state of equilibrium resurfacing, with new surface being produced in ~138,000 km^2 patches, with larger patch sizes possible in the case of a more realistic "feathering out" of resurfacing processes. Nevertheless, Grosfils and Head (1996) have argued that equilibrium resurfacing is not likely to have occurred, based on observations of radial dike swarms. Price *et al.* (1996) offer one possible resolution, noting that resurfacing in small scattered regions yields a crater population indistinguishable from random. Hauck *et al.* (1997) and Price (1997) have extended this work, and suggest that the portions of the surface of Venus may be currently undergoing modification. Previously (DeLaughter and Jurdy 1997), we showed that it is possible to assess corona-associated volcanism and tectonism by comparing impact crater density and modification out to four radii with that for random regions and that as much as 50% of the surface of Venus may have been affected.

The relative age of Venus' surface is typically estimated from impact crater density. Of the various mechanisms for the removal of impact craters (e.g., tectonism, embayment by exterior lavas, burial by surficial processes, and erosional degradation), only tectonism and volcanism are likely to be effective on the surface of Venus. Phillips *et al.* (1992) suggested that tectonism may be as effective as volcanism at removal of impact craters on the surface of Venus. In this paper, we investigate the potential of coronae for resurfacing.

0019-1035/99 $30.00

Coronae are abundant circular to elongate volcano-tectonic features on the surface of Venus which vary from 60 to 2600 km with an average diameter of 230 km. They consist of a central plateau, surrounded by an annular ring of ridges and troughs and typically include extensive exterior volcanism and tectonism (Stofan *et al.* 1992).

In their analysis of coronae, Stofan *et al.* (1992), divided the the 336 coronae and 26 "corona-like" features into seven categories based on Magellan SAR images and limited altimetry. The 17 Radial corona-like features, first identified with Magellan data, display domal topography with sets of radial fractures and troughs. The 9 Volcanic corona-like features include extensive radially lobate lava flows about gently sloping topographic highs, and sometimes possess radial faults, concentric faults or both. The majority of coronae (177) were classified as concentric, with symmetric, well-defined tectonic annuli. In 38 cases, two annuli were present and the coronae were classified as concentric–double ring. The presence of an interior low with raised annular rims and generally extensive interior volcanism was diagnostic of a concentric/caldera corona (8 members). The 17 radial concentric coronae possess interior radial faults and graben with an annular set of troughs and ridges and typically minimal volcanism. Sixty coronae had a marked asymmetry of form coupled with a sinuous annulus and were classed as asymmetric. If two or more coronae were linked with a continuous annulus and no evident age progression, the entire complex was classed as a multiple feature; interestingly, only 35 members were assigned to this class, even though we have found that 248 of the coronae have a separation less than the sum of their radii. In contrast, Watters and Janes (1995) noted that three generalized end-members can be isolated on the basis of topography: domes, plateaus, and depressions.

Corona evolution can be modeled as the interaction of a rising diapir with some boundary layer. This model predicts a variation in corona-associated volcanism and tectonic deformation throughout the evolution of the feature. During the initial domal uplift, radial fractures are formed; during this stage, volcanism is limited to the corona interior. This initial stage is followed by a flattening of the interior and development of an annular moat during which volcanism becomes prevalent outside the corona interior. Corona evolution terminates with the formation of a central caldera (Stofan and Head 1990, Janes *et al.* 1992, Stofan *et al.* 1992, Koch 1994). Koch and Manga (1996) estimated that it would take 50 myr for a 100-km-radius diapir to evolve from an initial uplift to a caldera. Coronae may be a major mode of heat transport on Venus (Phillips and Malin 1983). In addition, lithospheric thickness should constrain the interaction of a diapir with the surface. An understanding of corona evolution could thus clarify the wider issues of lithospheric thickness and the modes of heat transport, as well as resurfacing rates on Venus.

The applicability of the diapir model may not be evident from SAR images of coronae with widely different sizes due to the lack of a common scale. Normalization of the altimetry data by the corona radius obviates this problems, giving a simple ratio of the interior to exterior regions and mapping the effects from coronae of different radii onto a single scale. A simple scaling parameter has also been used to describe many geological processes involved in corona formation (e.g., heat flow, lithospheric flexure, diapiric rise) over a wide range of scales with a single set of equations. Previous researchers (e.g., Koch 1994) have normalized corona profiles using the radius as a scaling parameter for both the distance from the center and relief. Therefore, we investigate the normalized altimetry of the corona data set, and attempt to use it to quantitatively classify coronae. When normalized, we show that many coronae classified as different types by Stofan *et al.* (1992) have strikingly similar morphologies. In this paper, we present our classification and explore the implied age progression using impact crater statistics. By establishing the relative ages of these corona classes and the timing of their volcanism and tectonism, we may infer their potential for resurfacing.

2. CLASSIFICATION METHODOLOGY

We obtained the Magellan altimetry records for all orbits and filtered them to remove spurious data points. These data were then gridded at a 0.05° interval over the entire globe. Circular regions out to four corona radii were extracted from this grid. The extracted altimetry was normalized by feature radius by the following process: distances relative to the corona center were divided by the radius to give a normalized distance and normalized relief was found by dividing the relief relative to the lowest point by corona radius. As an example, for the corona Fatua (Fig. 1b), with a radius of 155 km, a point 310 km to the north and 310 km to the west of its center has normalized coordinates of (2, −2). Similarly, an actual relief of 3.1 km would correspond to a normalized relief of 0.02. Feature radius was taken from the appropriate list as described below.

3. CLASS CHARACTERISTICS

We have analyzed 394 features, including 358 from the Stofan *et al.* (1992) data set, 27 additional features taken from the USGS-Flagstaff data base (1996), and 9 taken from Magee Roberts and Head (1993). We characterize coronae with three shapes (domal, circular, and calderic; Table I). Two morphologies not related to coronae are also present (radial and volcanic; Table I).

TABLE I
Feature Distribution

Calderic	188	48%
Circular	93	24%
Domal	54	14%
Radial	28	6%
Volcanic	9	4%
Uncertain	22	6%

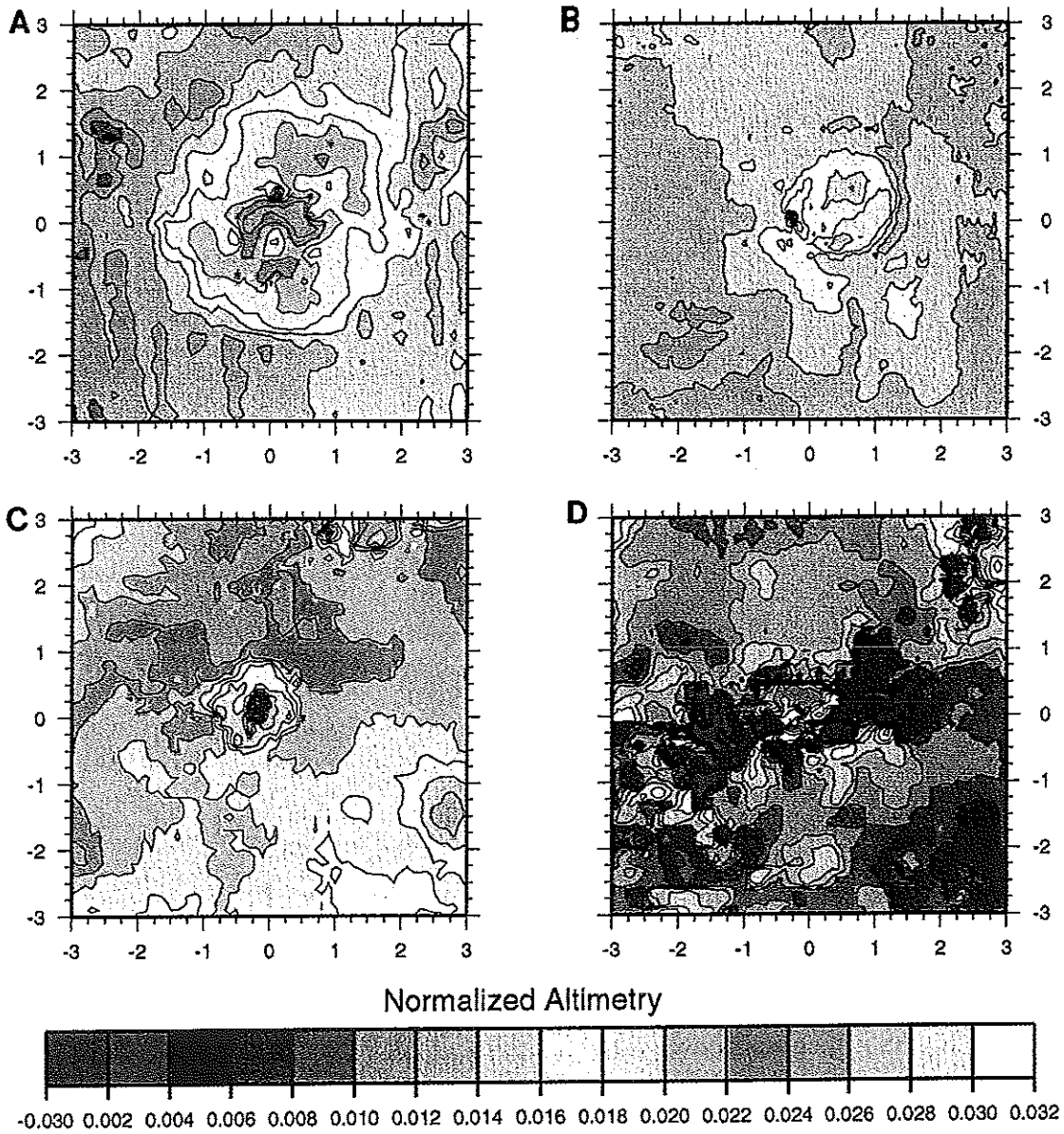

FIG. 1. Corona classes. (A) Domal corona Ninhursag, 38.0°S 270.0°E, 100 × 62.5 km. (B) Circular corona Fatua, 16.5°S 17.2°E, 155 × 155 km. (C) Calderic corona Teteoinnan, 38.5°S 149.5°E, 90 × 90 km. (D) Radial feature Oduduva, 11.0°S 211.5°E, 87.5 × 87.5 km. Distances are normalized by feature radius.

Variation between the corona shapes is gradational (Fig. 2) and reflects the developmental sequence of Koch and Manga (1996). Domal coronae (Fig. 1a) are distinguished by a central uplift with no surrounding moat. As Figs. 2a and 3 show, features which had been classed variously as radial concentric, concentric–double ring, concentric, and asymmetric by Stofan *et al.* (1992), display a domal morphology. These features may have associated radial fracturing, which, due to the low resolution of the altimetry data, is typically visible only in the SAR images. Fifty-four (14%) coronae have been classified as Domal. These features have a log-normal distribution of diameters, with a mode of 175–225 km (Fig. 4). They are noticeably clustered within the BAT region, along the trend of the chasmata. This may imply that there may be a genetic link between these coronae and rifting. Alternatively, it may be partly due to observational bias; many features have been identified variously as "novae" (Squyres *et al.* 1992), "arachnoids" (Head *et al.* 1992), and "Radial Concentric coronae" (Stofan *et al.* 1992). Since we have analyzed only the latter data set, it is possible that many more Domal coronae lurk on Venus. Several clear end-member examples of the Domal morphology exist (Fig. 3), as well as gradational forms with Circular coronae.

We arbitrarily distinguish the 93 (24%) Circular coronae (Fig. 1b) by the presence of a flattened interior and an annular moat, including features classed by Stofan *et al.* (1992) as multiple, radial concentric, concentric–double ring, concentric,

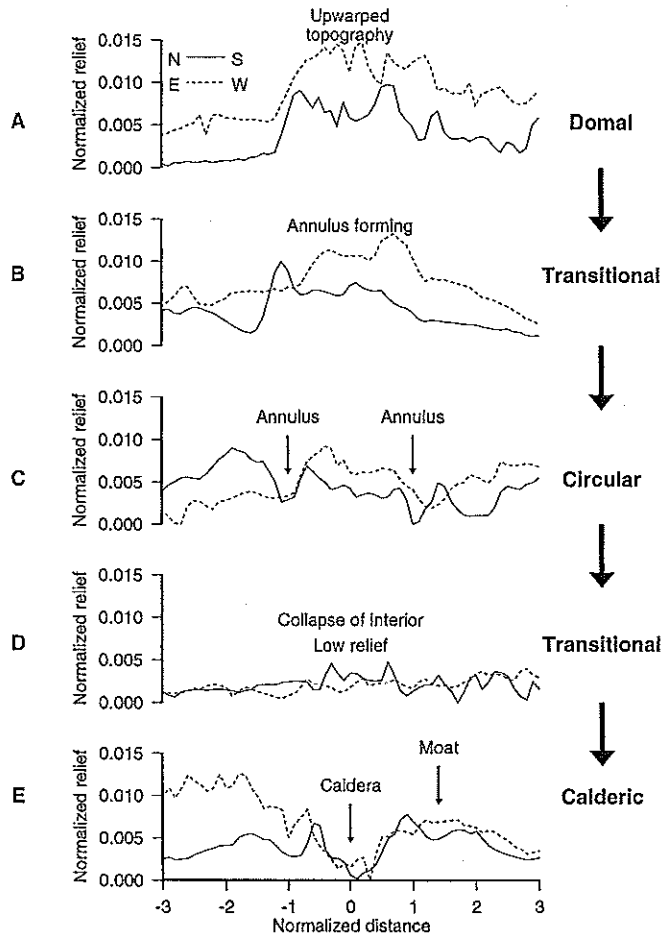

FIG. 2. Evolution of corona morphology. (A) Domal corona Selu 42.50°S 6.00°E, 150.00 km. (B) Transitional corona Earhart 71.00°N 136.00°E, 185.50 km. (C) Circular corona Kuan-Yin 4.30°S 10.00°E, 125.00 km. (D) Transitional corona Demeter 55.00°N 295.00°E, 333.50 km. (E) Calderic corona Holde 53.50°N 155.00°E, 100.00 km. A corona begins as a domal feature with radial fracturing and limited volcanism (domal stage). An annular moat forms and exterior volcanism dominates (circular stage). The corona center then collapses and volcanism is again restricted to the interior (calderic stage). The forms are gradational, with clear end-members in the domal and calderic stages. (Solid lines are N–S profiles through corona centers; dashed are E–W. Distances are normalized by feature radius.)

and asymmetric (Fig. 5). Some portions of their interiors may be lower than the surrounding plains. In SAR images, these typically have concentric fractures and more well-defined lava flows. The circular coronae are not as obviously clustered as the domal (Fig. 1d), with a more gaussian distribution of sizes and a mode of 275–325 km (Fig. 6).

Calderic coronae (Fig. 1c) are those with more than 50% of the interior significantly lower than the surrounding plains. They sometimes possess raised rims and annular moats; in SAR images, they are surrounded by degraded lava flows which are often indistinguishable from surrounding plains deposits. We identify 188 (48%) calderic coronae, whereas Stofan *et al.* had only assigned 9 (2%) concentric caldera coronae; consequently, members of their concentric, asymmetric, and multiple morphologies fall into our calderic class (Fig. 7). These coronae have a clear leg-normal size distribution, with a mode of 125–175 km (Fig. 8). The members of this class are widely distributed, with the smallest members clustered in the BAT region. There exists a spectrum of shapes between the circular and the typical end-member calderic morphologies.

Some remaining features distinctly differ from coronae. We identify 28 radial features (Fig. 1d), with a domal to flat topography, multiple calderas, and evidence of lineament-related volcanism in scattered locations, consistent with characteristics identified as diagnostic of giant radiating dike swarms on Venus (Head *et al.* 1992, Magee Roberts and Head 1993, Grosfils and

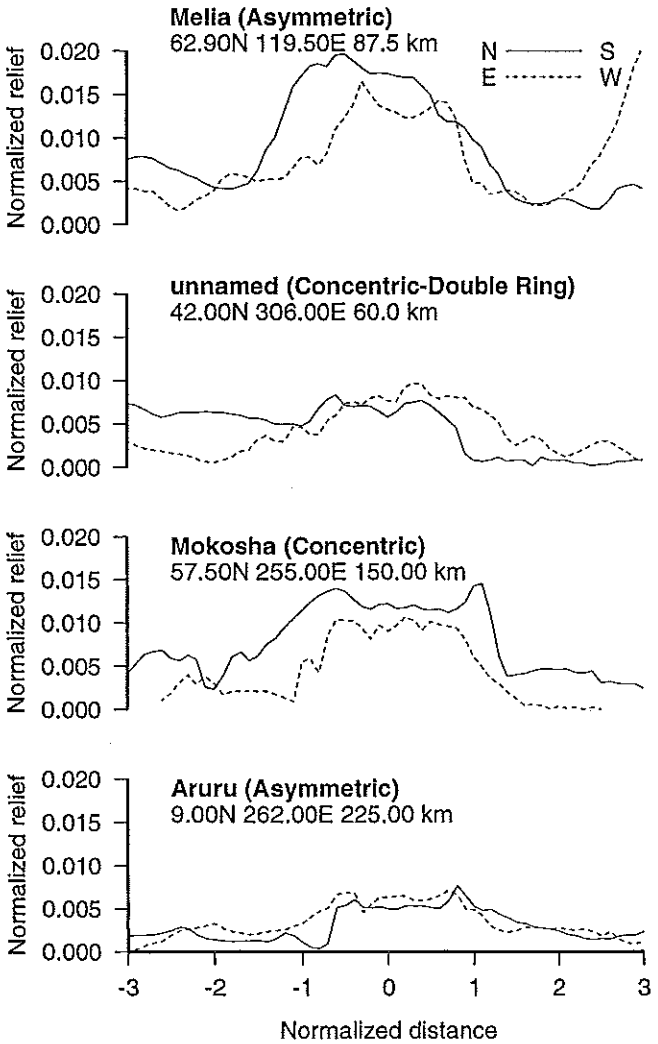

FIG. 3. Domal coronae (Stofan *et al.* classification in parentheses). End-members of the domal corona class. These features show marked similarities, even though they vary from 60 to 225 km. Domal features are distinguished by a central uplift with no surrounding moat. They may have associated radial fracturing which is typically visible only in SAR images. (Solid lines are N–S profiles through corona centers; dashed are E–W. Distances are normalized by feature radius.)

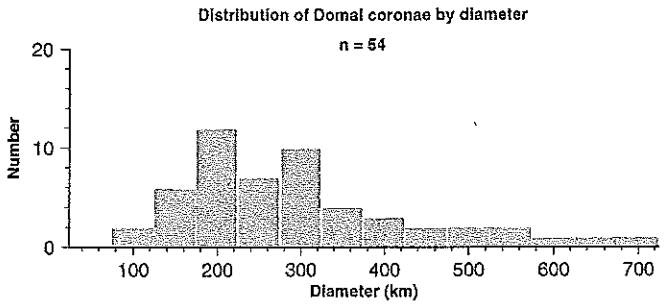

FIG. 4. Distribution of domal coronae by diameter. These features have a log-normal distribution, with a mode of 175–225 km, and a secondary peak from 275 to 325 km. We have identified 54 domal coronae; however, many more domal coronae may lurk on Venus due to classification of features variously as "novae". (Squyres *et al.* 1992), "arachnoids" (Head *et al.* 1992), and "Radial Concentric coronae" (Stofan *et al.* 1992).

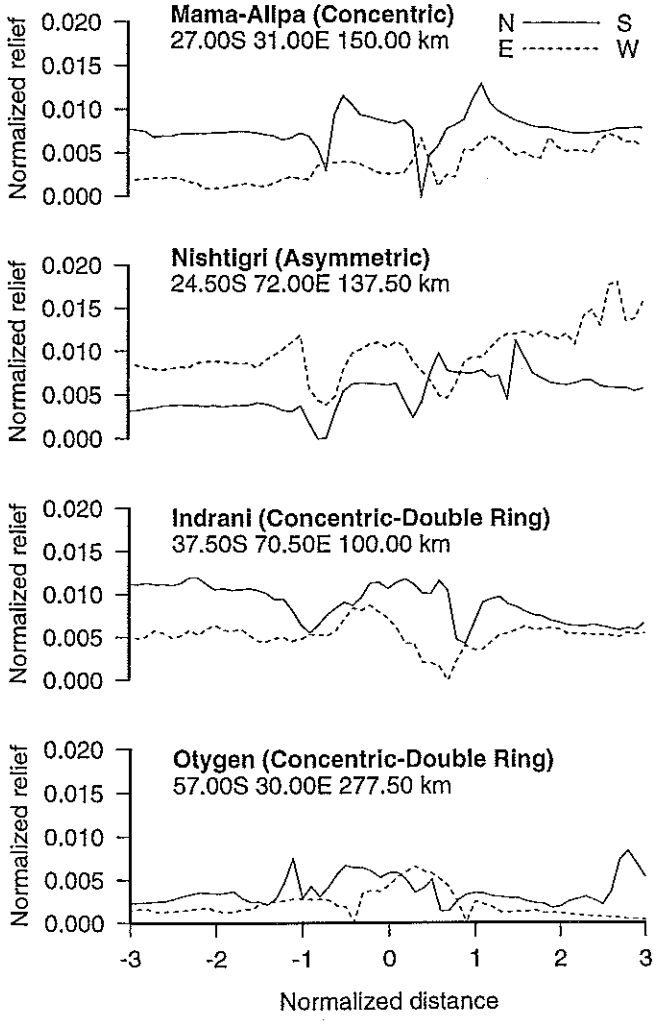

FIG. 5. Circular coronae (Stofan *et al.* classification in parentheses). Circular coronae are distinguished by a flattened interior and an annular moat. These coronae typically have concentric fractures and more well-defined lava flows evident in SAR images. These coronae often have forms gradational with the domal or calderic stages. (Solid lines are N–S profiles through corona centers; dashed are E–W. Distances are normalized by feature radius.)

Head 1994, DeLaughter and Jurdy 1997). We classify a further 9 features as volcanic, based on broad, sloping flanks, with evidence of extensive lava flows in SAR images. A residual 22 (6%) features were unclassifiable, due to problems with the Magellan altimetry data set.

4. IMPACT CRATER STATISTICS

Normalized-radius classification makes testable predictions about corona age and related processes, such as tectonism and volcanism. During the domal phase, tectonism dominates with volcanism limited to the corona interior. The circular stage features prevalent exterior volcanism and continued tectonism. The calderic stage should undergo a decrease in tectonism and volcanism as the corona senesces. Thus, each stage should interact with the surrounding terrain in a unique fashion. These effects would be seen best in a detailed stratigraphic analysis (e.g., Ivanov and Head 1998, Basilvesky 1998), but such an analysis is beyond the scope of this preliminary study. Therefore, we examine impact crater statistics near coronae and take as the null hypothesis that impact crater populations will not differ from the global mean.

We compare impact crater populations within three radii of actual coronae with those for Monte Carlo simulations of corona location. Since some models predict that the amount of time

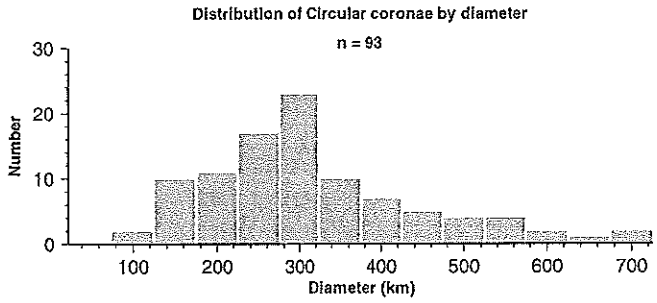

FIG. 6. Distribution of circular coronae by diameter. These features have a gaussian distribution, with a mode of 275–325 km. We have identified 93 circular coronae.

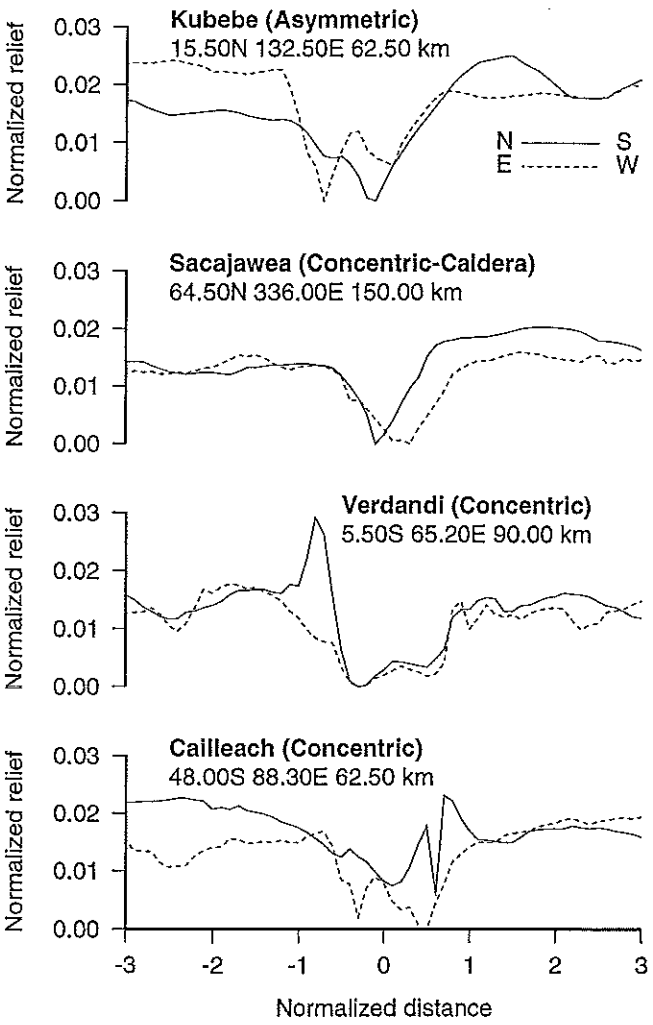

FIG. 7. Calderic coronae (Stofan *et al.* classification in parentheses). End-members of the calderic coronae. These features have more than 50% of the interior significantly lower than the surrounding plains and sometimes possess raised rims and annular moats. SAR images show degraded lava flows which are often indistinguishable from surrounding plains deposits. (Solid lines are N–S profiles through corona centers; dashed are E–W. Distances are normalized by feature radius.)

spent in each stage depends on corona size, we perform comparisons of coronae with diameters 275–325 km, as well as the entire set.

Phillips and Izenberg (1994, pers. commun.) have identified 940 impact craters on the surface of Venus, of which 654 (69.6%) are pristine, 224 (23.8%) are possibly tectonized, and 138 (14.7%) are possibly embayed (76 may be both tectonized and embayed). Variations of impact crater populations provide a measure of surface age (Phillips *et al.* 1992). For a uniform age, then the impact crater densities and proportion of modified craters near any feature set would be similar to global averages. If the surface varies in age, then for a set of young features the proportion of modified craters should be significantly greater than the global average, whereas the crater density should be lower than the global average. Alternatively, near older features the proportion of modified craters should be lower than the global average, with a higher crater density. Price *et al.* (1996) put forth a similar argument in their comparison of stratigraphic with crater statistic data.

5. METHODOLOGY

To a first approximation, impact craters are randomly distributed on the surface of Venus and exhibit local concentrations or deficits due to stochastic variation (Phillips *et al.* 1992, Schaber *et al.* 1992); however, examination of modified craters shows that they are not randomly distributed (Price 1997). Thus, by using a combination of impact crater density and proportion of modified craters, we can derive a measure of the amount of resurfacing in a region (Price *et al.* 1996, Price 1997).

Here we compare the impact crater density and proportions of tectonized and embayed craters within three corona radii with the expected "background" level. We use Monte Carlo simulations to determine the variance and mean expected in impact crater statistics for each of the classes studied. A trial for each class uses the number and diameters of the actual coronae but with randomly chosen locations (e.g., 11 data points for the trials simulating the size-restricted domal corona data set). Random locations for simulated corona sets were generated with a gaussian distribution in spherical coordinates. One thousand trials constitute the Monte Carlo simulation for each class.

For each Monte Carlo simulation, we calculate the mean and variance of the proportion of tectonized and embayed craters and crater density. Observed significance levels (i.e., the probability that the result is nonrandom) for each class are found from the binomial approximation. The Monte Carlo simulations have impact crater densities and proportions of tectonized and embayed craters which are very close to those found in the global crater data set, suggesting that no systematic bias is present. Because of this high degree of similarity, we perform Monte Carlo simulations only for the size-restricted subsets and apply these results to each class.

Even though many analyses have found a nonrandom distribution of these features (e.g., Stofan *et al.* 1992, Squyres *et al.*

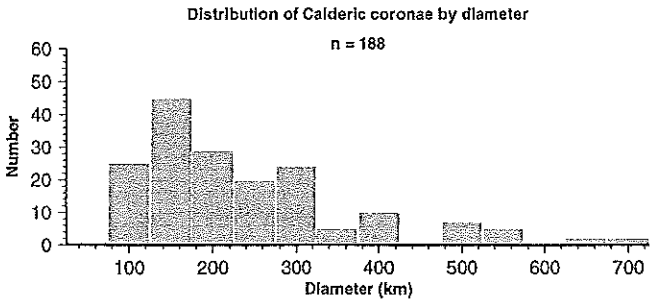

FIG. 8. Distribution of calderic coronae by diameter. These features have a log-normal distribution, with a mode of 125–175 km. We have identified 188 calderic coronae.

TABLE II
Search Region Areas

	Area	Monte Carlo	Significance (%)
Calderic	14.8	14.6 ± 0.5	68
Circular	16.0	16.5 ± 0.6	77
Domal	6.9	6.9 ± 0.2	50

Note. Areas in 10^6 km^2 for regions surrounding coronae with diameters from 274 to 325 km. "Monte Carlo" are simulation results. Impact crater data is from Phillips and Izenberg (1994, pers. commun.). Corona data is from Stofan *et al.* (1992), USGS (1996), and Magee Roberts and Head (1993) data sets.

1993, Stefanick and Jurdy 1996, Nagasawa *et al.* 1997), the search area around each corona subset closely approximates that found from the Monte Carlo simulations. For all corona classes, a search radius of three corona radii provides search regions greater than 5×10^6 km^2 (Table II), the minimum needed to generate statistically robust crater counts (Phillips *et al.* 1992).

6. RESULTS

Impact crater statistics for the size-restricted corona classes suggest an age progression from domal through circular to calderic. The 24 calderic coronae with diameters between 275 and 325 km have an associated impact crater population very similar to the global mean (Table III), though with slightly too few tectonized craters. Many of the features in this class are associated with extensive lava flows; for example, Willis and Hansen (1995) found that as much as 20% of Lakshmi Planum had been covered by lobate lava flows traceable to one corona. Thus, to reconcile extensive lava flows with an unperturbed crater population, we infer that the calderic coronae are older than the average surface and are no longer active.

TABLE III
Impact Crater Populations for Size-Restricted Coronae

	Craters	Monte Carlo	Significance (%)
Calderic coronae ($n = 24$)			
Total	30	30.4 ± 5.6	56
Tectonized	5	7.3 ± 1.2	81
Embayed	3	4.5 ± 1.0	75
Circular coronae ($n = 27$)			
Total	23	32.2 ± 5.9	96
Tectonized	7	5.8 ± 0.9	80
Embayed	3	3.6 ± 0.8	61
Domal coronae ($n = 11$)			
Total	10	14.15 ± 3.7	87
Tectonized	4	2.4 ± 0.6	89
Embayed	1	1.5 ± 0.5	69

Note. As in Table II; all coronae in each class were used.

The 27 circular coronae with diameters between 274 and 325 km have a low impact crater density and a slightly elevated proportion of tectonized craters (Table III). The percentage of embayed craters reaches the global mean. Therefore, we infer that circular coronae are currently active.

The 11 domal coronae with diameters between 275 and 325 km have fewer than the expected number of impact craters, of which more are tectonized than expected (Table III); however, the number of embayed craters approximates the expected values. This is consistent with Squyres *et al.* (1992) who found evidence of early radial fracturing extending beyond the corona interior. Thus, we infer that surface modification has begun, but is not yet effective at removal of craters.

7. DISCUSSION

Our analysis highlights several facets of corona formation and evolution. The most important of these is that coronae may be classified using altimetry data which has been scaled to the feature by its radius. The resulting classification is both simpler than that previously used and more directly reflects models of corona formation (e.g., Stofan and Head 1990, Janes *et al.* 1992, Stofan *et al.* 1992, Koch 1994). As expected from the models, corona types are gradational with a few clear end-members. Interestingly, we find that many more of the coronae are in an apparently terminal stage of development than was suggested by Stofan *et al.* (1992).

A model-based classification of coronae also provides testable predictions about their evolution and effects. A detailed stratigraphic analysis would provide a better measure of corona ages and effects relative to their surrounding terrains than impact crater population statistics, but such an analysis is beyond the scope of this preliminary study. One weakness of the analysis used here is that it tacitly assumes that coronae interact with the surrounding terrains rather than being independent entities. Given that Cyr and Melosh (1993) demonstrated that tectonic deformation may extend as far as three corona radii from the center, and Magee Roberts and Head (1993) have shown that 41% of the coronae in their data set possess lava fields extending two to three radii, we feel that the interaction of coronae with the surrounding terrain is well documented.

The predictions of the diapiric model are not invalidated by impact crater populations near a size-restricted set of coronae. However, taking each corona class as a whole and examining the corresponding impact crater population (Table IV) demonstrates the effect of size. For example, there is a deficit of impact craters near all Calderic coronae, where the size-restricted subset had the expected number. This effect may have several causes. First, the rate at which a corona evolves from the domal to the calderic stages may depend on the feature size, as suggested in some models (e.g., Koch and Manga 1996). Second, the approximation of the venusian crater record as being spatially random has been shown to be incorrect (Price *et al.* 1996, Price 1997); thus, it may be necessary to use more sophisticated modeling techniques to

TABLE IV
Impact Crater Populations for All Class Members

	Craters	Monte Carlo	Significance (%)
Calderic coronae ($n = 188$)			
Total	257	367.8 ± 67.1	96
Tectonized	51	62.0 ± 10.3	70
Embayed	23	37.7 ± 8.4	80
Circular coronae ($n = 93$)			
Total	136	152.5 ± 26.4	62
Tectonized	38	32.3 ± 5.2	70
Embayed	19	20.3 ± 4.3	56
Domal coronae ($n = 54$)			
Total	72	89.7 ± 23.3	78
Tectonized	18	17.4 ± 4.6	50
Embayed	10	10.9 ± 3.8	55

Note. As in Table II; all coronae in each class were used.

estimate the relative ages of the coronae. Third, clustering of coronae, which may be at least partially size-dependent, may modify their effects on surrounding regions. It is likely that this question will be resolved only by detailed stratigraphic analyses.

Independent support for a model-based classification of coronae is given by the correlation of domal features with geoid highs (Jurdy and Stefanick 1999), implying that they are young, active features. In their study of flow fields, Magee Roberts and Head (1993) found evidence for younger coronae to be larger, with an increased association with rifting. We find that the largest of the domal coronae strongly cluster within the BAT region, which may be a region of major upwelling within Venus (Crumpler *et al.* 1993). If this is true, then BAT may be analogous to Tharsis Regio on Mars, which has been modeled as a long-lived plume (Harder and Christensen 1996).

8. CONCLUSIONS

We develop a corona classification scheme using normalized topography, in addition to SAR imagery. Scaling topography by radius, we find that coronae which have been assigned to different classes by Stofan *et al.* (1992) show striking similarities of shape and relief. We have identified a few basic corona shapes (domal, circular, and calderic) which may reflect the evolutionary stages of diapiric evolution (early, middle, and late).

This classification makes testable predictions about the age and sequence of events in corona evolution. These predictions are not invalidated by impact crater populations near coronae, though the inherent uncertainties in this form of analysis makes any conclusions tentative at best. The domal features (impact crater density 1.45×10^{-6} km^2) appear emergent; tectonism dominates this stage and continues into the next. With the lowest impact crater density (1.43×10^{-6} km^2), circular coronae seem currently active. The calderic features (impact crater density 2.03×10^{-6} km^2) are in the terminal stage and so have little effect on the surrounding regions, despite their active past evidenced by the extensive associated lava flows. Finally, the effects of corona activity extend well beyond the interior into the surrounding terrain.

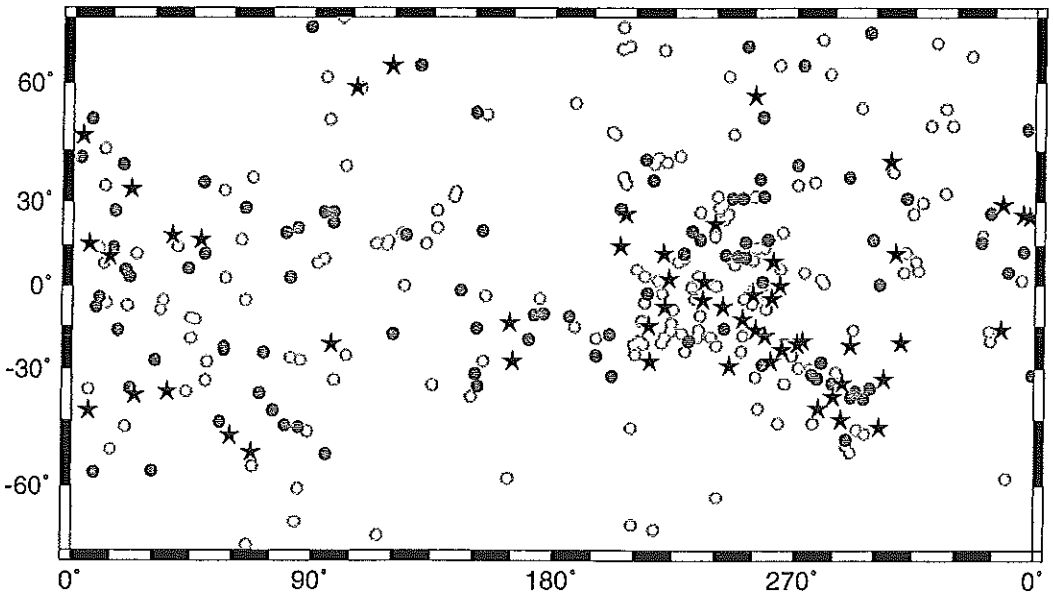

FIG. A1. Distribution of coronae by type. Mercator projection with location of coronae. The 54 domal coronae (Black stars) are distinguished by a central uplift with no surrounding moat. The 93 circular coronae (filled gray circles) are distinguished by a flattened interior and an annular moat. The 188 calderic coronae (hollow gray circles) have more than 50% of the interior significantly lower than the surrounding plains and sometimes possess raised rims and annular moats. Feature locations and diameters are taken from Stofan *et al.* (1992), Magee Roberts and Head (1993), and the USGS (1996) corona data sets.

TABLE A1

Corona Classified by Evolutionary Stage

Lat	Long	Diameter (km)	Shape	Class	Name
79.0	300.0	437 x 282	CIR	CONC	Pomona
77.0	278.0	430 x 340	CIR	CONC	Anahit
77.0	204.0	241 x 205	CIR	CONC	Maslenitsa
75.2	220.0	100	CAL	CONC	
74.0	214.0	150	CAL	CONC	
73.0	260.0	653 x 391	DOM	ASYM	Bachue
71.0	136.0	370	CIR	CONC	Earhart
70.0	101.0	284 x 188	CAL	ASYM	Tusholi
68.8	89.0	183	CIR		Ops
68.7	205.7	140	CAL		Nzingha
68.0	298.0	217 x 195	CIR	CONC	Otau
67.0	280.0	435 x 352	CAL	ASYM	Feronia
66.5	323.0	225 x 175	CAL	C-CAL	Colette
66.0	252.0	350 x 250	CIR	MULT	Upunusa
66.0	208.0	200 x 160	CAL	MULT	Semele
65.6	205.4	163	CAL		Muzamuza
65.5	221.0	125	CAL	CONC	
64.5	336.0	300	CAL	C-CAL	Sacajawea
63.0	273.0	335 x 296	CIR	ASYM	Coatlicue
63.0	264.0	503 x 435	CAL	CONC	Rananeida
63.0	130.0	560 x 480	CIR	CONC	Nightingale
62.9	119.5	175	DOM	ASYM	Melia
61.5	283.0	225	CAL	C-DR	
61.1	245.0	150	CAL	CONC	
61.0	95.0	690 x 430	CAL	ASYM	Vacuna
59.0	108.0	320 x 300	CAL	ASYM	Fakahotu
59.1	106.4	290	DOM		
57.5	255.0	300 x 150	DOM	CONC	Mokosha
56.0	188.0	200	CAL	ASYM	
55.0	295.0	667 x 333	CAL	CONC	Demeter
54.8	326.5	180	CAL	ASYM	
54.0	21.8	375 x 260	RAD	RAD	Haumea
54.0	151.0	200	CIR	ASYM	
53.5	155.0	200	CAL	CONC	Holde
53.0	258.0	515 x 480	CIR	CONC	Bau
53.0	150.9	100	RAD		Ciuacoatl
52.7	6.8	303	CIR		Nepret
52.6	306.5	600	CIR	MULT	Beiwe
52.5	96.5	120	CAL	CONC	
51.0	329.0	380 x 267	CAL	CONC	
51.0	321.0	300	CAL		Xilonen
50.2	357.0	300	CIR	ASYM	Ashnan
49.6	201.8	217	CAL		Cerridwen
49.0	247.0	380	CAL	CONC	
49.0	203.0	225 x 210	CAL	MULT	Neyterkob
48.8	3.5	280	DOM	ASYM	Onatah
48.3	0.3	300 x 190	CAL	CONC	
45.5	12.0	225	CAL	ASYM	Audhumla
43.5	227.0	300	CAL	CONC	
43.2	2.7	160	CIR	CONC	Vasudhara
43.0	219.0	270	CAL	MULT	
42.5	214.3	250 x 150	CIR	MULT	
42.0	306.0	120	DOM	C-DR	
41.7	222.0	160	CAL	CONC	
41.5	288.0	900	RAD	RAD	
41.4	217.5	180	CAL	C-DR	
41.2	19.0	175	CAL	CONC	
41.0	271.0	274 x 263	CIR	C-DR	Rauni
40.8	102.5	300	CAL	ASYM	Maan-Eno
39.0	307.0	120	CAL	C-DR	
38.0	36.5	180	VOL	C-DR	
37.5	67.5	175	CAL	CONC	Olwen
37.5	290.5	150	CAL	CONC	
37.5	206.0	180	CAL	CONC	
37.0	257.0	400	CIR	CONC	Junkgowa
36.5	217.0	300	CIR	ASYM	
36.0	49.0	500 x 225	CIR	ASYM	Nefertiti
36.0	277.5	125	CAL	MULT	
35.5	207.0	150	CAL	CONC	
35.0	293.5	300 x 225	UNC	MULT	Blathnat
35.0	271.0	160	CAL	CONC	
35.0	12.0	320	CAL	CONC	

TABLE A1—*Continued*

Lat	Long	Diameter (km)	Shape	Class	Name
34.0	22.0	200	DOM	RAD	Lilinau
33.5	57.0	150	CAL	CONC	Kayanu-Hime
33.0	143.5	300	CAL	CONC	
32.7	326.5	200	CAL	C-DR	Renenti
31.5	258.5	320	CIR	CONC	
31.5	255.0	300	CAL	CONC	
31.5	241.0	385 x 330	CAL	CONC	
31.5	142.9	553	CAL		Cauteovan
31.0	312.0	225	CIR	C-DR	
31.0	250.5	200	CAL	CONC	
31.0	246.5	162	CIR	MULT	
29.5	318.0	300	CAL	CONC	
29.0	348.0	180	DOM	RAD	
29.0	243.0	200	CAL	CONC	
28.0	65.0	300 x 225	CIR	ASYM	Umm Attar
28.0	241.5	100	CAL	VOLC	
25.7	245.0	132	CAL	ASYM	
27.5	205.0	230	CIR	CONC	
27.0	342.6	190	RAD	RAD	Mesca
27.0	16.0	290	CIR	ASYM	Beyla
27.0	136.5	300	CAL	CONC	Boann
26.5	98.0	225	CIR	CONC	Anquet
26.5	94.5	200	CIR	C-DR	Eurynome
26.5	33.0	110	RAD	RAD	
26.5	234.5	125	CAL	CONC	
26.1	343.5	170	CAL	CONC	Purandhi
26.0	314.5	290	CAL	CONC	
25.8	207.0	250 x 160	DOM	ASYM	
25.5	355.5	300 x 200	DOM	CONC	Nissaba
25.0	358.0	230	DOM	CONC	Idem-Kuva
24.5	264.0	280	RAD	VOLC	
24.0	243.5	500 x 225	CAL	MULT	
23.5	218.5	145	VOL	ASYM	
23.0	98.0	225	CIR	CONC	Maya
22.5	256.7	150	UNC	ASYM	
22.5	240.0	150	DOM	CONC	
22.0	224.0	350	RAD	R-CON	
21.0	84.5	320	CIR	VOLC	Erishkigal
21.0	136.5	400	CAL	CONC	Kamadhenu
20.0	231.5	325	CIR	CONC	
20.0	153.5	225 x 150	CAL	CONC	
19.5	265.5	150	CAL	CONC	
19.5	227.5	350	RAD	R-CON	
19.3	80.1	200	CIR	VOLC	Kunhild
19.2	123.5	75	CAL	CONC	
18.5	37.5	320	DOM	CONC	
18.5	125.0	250	CIR	CONC	Abundia
18.3	340.5	150	CAL	CONC	Chiun
18.0	240.0	125	CAL	CONC	
17.8	240.0	350 x 300	RAD	CONC	
17.0	63.5	100	CAL	CONC	
17.0	48.0	750 x 350	DOM	CONC	
17.0	260.0	370	CIR	VOLC	
17.0	234.5	500	CIR	R-CON	Perchta
17.0	299.5	250	CIR	CONC	
16.5	118.5	200 x 150	CAL	CONC	Omeciuatl
16.0	340.0	310	CIR	ASYM	Benten
16.0	311.3	80	VOL	C-CAL	
16.0	251.5	525	CIR	ASYM	Taranga
15.5	6.0	120	DOM	CONC	
15.5	132.5	125	CAL	ASYM	Kubebe
15.5	114.0	150	CAL	CONC	Allatu
15.0	118.0	125	CAL	CONC	Bhumiya
14.5	39.5	500	CAL	CONC	
14.5	205.0	200	DOM	CONC	
14.5	111.7	100	UNC	CONC	Dhisana
14.2	15.4	300	CIR	CONC	Sappho
14.0	258.8	125	CAL	CONC	
14.0	256.5	180 x 125	CAL	CONC	
14.0	254.5	125	CAL	CONC	
14.0	10.0	345	CAL	ASYM	Nehalennia
13.5	253.0	200	UNC	CONC	
13.0	226.5	300	UNC	MULT	

TABLE A1—*Continued*

Lat	Long	Diameter (km)	Shape	Class	Name
12.6	355.7	270	CIR		Silvia
12.3	311.8	100	CAL	CONC	
12.0	49.5	540	CIR	CONC	
12.0	308.0	300	DOM	CONC	
12.0	24.0	350	CAL	CONC	Liberia
12.0	228.5	250	CIR	ASYM	
12.0	221.0	850 x 450	DOM	ASYM	Zisa
11.5	244.0	290	CIR	C-DR	
11.0	248.5	300	CIR	CONC	
11.0	14.0	240	DOM	VOLC	Anaia
10.5	251.5	300	CIR	CONC	
10.0	94.7	120	CAL	CONC	
10.0	246.0	200	CAL	C-DR	
10.0	228.5	150	CAL	C-DR	
9.5	254.5	150	CAL	C-DR	
9.0	68.0	150	RAD	RAD	H'ururu
9.0	315.5	200	CAL	CONC	
9.0	262.0	450 x 350	DOM	ASYM	Aruru
9.0	226.5	100	CAL	CONC	
8.5	92.0	150	CAL	CONC	Atse Estsan
8.3	11.7	170	CAL	CONC	Sunrta
8.0	247.5	150	CAL	CONC	
7.5	313.5	90	UNC	CONC	
6.5	43.5	575	CIR	C-DR	Calakomana
6.2	264.7	75	CAL	CONC	
6.0	211.0	60	CAL	CONC	
6.0	21.5	400	UNC		Gaia
6.0	20.0	300	CIR	CONC	Belet-ili
5.5	316.5	250	CAL	MULT	
5.5	313.0	100	UNC	CONC	
5.5	226.0	450 x 300	UNC	MULT	
5.0	350.0	375	CIR		Eingana
5.0	311.0	150	CAL	CONC	
5.0	273.7	375 x 200	CAL	MULT	
3.5	233.7	225	CAL	CONC	
3.5	214.0	150 x 125	CAL	CONC	
3.5	21.5	400	CIR	MULT	Gaia
3.0	81.8	125	CIR	CONC	Habonde
3.0	57.5	250 x 150	CAL	ASYM	
2.5	280.0	225 x 150	CAL	MULT	
2.5	223.0	525 x 300	DOM	ASYM	
2.0	355.0	1060	CAL	CONC	Heng-o
2.0	285.0	225	UNC		
2.0	219.0	85	CAL	CONC	
1.5	258.0	100	CIR	CONC	
1.5	236.0	450 x 250	DOM	MULT	
1.0	281.0	170	CAL	CONC	
0.5	302.0	675	CIR	CONC	
0.0	264.5	200	DOM	CONC	
0.0	240.5	125	CAL	CONC	
0.0	124.5	300	CAL	ASYM	Rosmerta
-0.4	134.5	125	RAD	RAD	Blai
-0.5	231.3	175	CAL	CONC	
-1.0	255.0	100	CAL	CONC	
-1.5	211.5	240	UNC	CONC	
-2.0	243.0	275 x 150	UNC	MULT	
-2.0	215.0	180	VOL	CONC	
-2.0	145.5	150	CIR	C-DR	Hepat
-3.0	220.5	150	CAL	CONC	
-3.0	215.0	300	CIR	C-DR	
-3.0	153.0	225	UNC	MULT	Seia
-3.5	259.5	275 x 150	CAL	MULT	
-3.5	254.5	325	DOM	CONC	
-4.0	210.5	260 x 200	UNC	CONC	
-4.0	154.8	150	CAL	CONC	
-4.3	10.0	250	CIR	CONC	Kuan-Yin
-5.0	261.5	300 x 150	DOM	MULT	Krumine
-5.0	251.0	500	CAL	ASYM	
-5.0	232.5	125	CAL	CONC	
-5.0	175.0	200	CAL	CONC	Eigin
-5.5	65.2	180	CAL	CONC	Verdandi
-5.5	34.0	190	CAL	C-DR	
-5.5	235.5	150	DOM	CONC	

TABLE A1—*Continued*

Lat	Long	Diameter (km)	Shape	Class	Name
-6.5	214.0	175	CAL	CONC	
-6.5	12.9	290	CAL	C-CAL	Thouris
-7.0	254.2	100	CAL	CONC	
-7.5	20.7	480	CAL	CONC	Cybele
-8.0	8.6	410	CIR	ASYM	Atargatis
-8.0	243.0	350 x 260	DOM	R-CON	
-8.0	221.5	600 x 300	DOM	ASYM	
-8.5	47.0	525	UNC	R-CON	Nabuzana
-8.8	259.3	100	CAL	CONC	
-9.0	33.0	330	CAL	CONC	Thermuthis
-9.0	214.0	275	RAD	R-CON	
-9.0	224.6	114	CAL	C-CON	
-10.5	176.5	450 x 360	CIR	ASYM	Sith
-11.0	211.5	175	RAD	R-CON	Oduduva
-11.0	173.0	300	CIR	R-CON	
-11.3	234.5	230 x 160	CAL	CONC	
-11.5	186.0	530	CIR	CONC	
-12.0	44.5	150	CAL	C-DR	
-12.5	261.5	170	VOL	VOLC	
-12.5	250.5	350 x 250	DOM	CONC	
-12.5	133.5	450	RAD	RAD	
-12.5	46.0	525	CAL		Mukylchin
-13.2	237.7	180	UNC	CONC	
-13.2	213.0	210	CAL	CONC	
-14.0	224.0	300	CAL	CONC	
-14.0	163.8	300	DOM	R-CON	Miralaidji
-15.0	215.5	220	DOM	R-CON	
-15.5	188.0	125	CAL	CONC	
-16.0	243.5	600 x 400	CIR	ASYM	
-16.0	151.5	675	CIR	CONC	Ceres
-16.3	351.2	200	VOL		Tumas
-16.4	347.5	180	DOM	MULT	
-16.5	292.0	100	CAL	CONC	
-16.5	255.5	180	DOM	CONC	
-16.5	234.0	290 x 225	CAL	MULT	
-16.5	17.2	310	CIR	C-DR	Fatua
-16.7	223.7	125	CAL	CONC	
-17.0	343.0	200	CAL	CONC	Bhumedevi
-17.7	227.8	100	CAL	CONC	
-18.0	201.0	150	CIR	C-DR	
-18.0	120.3	300 x 200	CIR	R-CON	Inari
-18.5	259.0	225	DOM	MULT	Nagavonyi
-18.5	250.5	200	CAL	C-DR	
-19.0	238.5	225	CAL	C-DR	Aeracura
-19.0	233.5	660 x 380	CAL	MULT	Beruth
-19.0	221.5	230	CAL	CONC	
-19.5	196.0	230	CAL	CONC	
-19.5	44.5	320	CAL		Juksakka
-19.6	345.3	125	RAD		Takus Mana
-20.0	171.0	870 x 750	CIR	C-DR	
-20.2	102.5	150	RAD	RAD	
-20.3	230.3	225	CIR	C-DR	
-20.5	343.5	150	CAL	CONC	Qetesh
-20.5	273.0	150	DOM	CONC	
-20.5	212.2	125	CAL	CONC	
-21.0	310.0	500	DOM	C-DR	Iweridd
-21.0	220.3	260	CAL	MULT	
-21.3	266.4	90	CAL	C-CAL	
-21.5	97.3	160	DOM	CONC	
-21.5	271.0	250 x 200	DOM	ASYM	
-21.5	213.5	225 x 100	CAL	MULT	
-21.7	210.2	100	CAL	CONC	
-22.0	291.0	400	DOM	CONC	
-22.0	240.5	220	CAL	C-DR	
-22.5	57.0	420	CIR		Ma
-23.5	57.0	450	CIR	CONC	
-23.5	265.3	375 x 320	DOM	ASYM	
-24.0	250.0	530 x 310	CAL	ASYM	
-24.0	229.0	225	CAL	MULT	
-24.0	157.5	275	RAD	RAD	Bona
-24.5	72.0	275	CIR	ASYM	Nishtigri
-24.5	177.3	150	RAD	RAD	
-25.0	210.5	100	CAL	CONC	

TABLE A1—*Continued*

Lat	Long	Diameter (km)	Shape	Class	Name
-25.5	269.0	250	CAL	C-DR	Hervor
-25.5	196.0	100	CAL	CONC	
-25.5	103.0	225	CAL	C-DR	
-26.3	82.0	350	CAL	C-CAL	Aramaiti
-27.0	85.7	175	CAL	CONC	Ohogetsu
-27.0	31.0	300	CIR	CONC	Mama-Allpa
-27.2	272.8	300	RAD	RAD	
-27.5	50.5	375	CAL	C-DR	
-27.5	261.2	225	DOM	CONC	
-27.5	216.0	200 x 145	DOM	C-DR	
-27.5	165.0	150	DOM	C-DR	
-27.5	154.0	200	CAL	C-DR	Mayaeul
-27.7	280.0	150	CIR	VOLC	
-28.0	270.0	200	RAD	R-CON	
-28.0	232.1	200	RAD	RAD	
-28.0	209.5	535 x 225	UNC	MULT	Epona
-28.5	258.0	240	CAL	CONC	
-28.7	258.0	200	CAL	CONC	
-29.0	245.5	420 x 225	DOM	MULT	
-29.2	282.5	166	VOL	CONC	
-29.5	271.5	500	CAL	ASYM	
-30.0	276.0	300	CAL	C-DR	Gertjon
-30.5	110.5	150	RAD	CONC	
-31.0	285.5	250	CAL	CONC	
-31.5	259.5	400	UNC	CONC	
-31.5	151.0	350	CIR	ASYM	Colijnsplaat
-31.7	276.5	300 x 225	CIR	ASYM	
-32.0	359.0	330	CIR	CONC	Eve
-32.3	202.0	150	CIR	CONC	
-32.5	95.0	175	CIR	ASYM	Tai Shan
-32.5	255.5	380 x 200	CAL	MULT	Oanuava
-33.0	278.5	300	CIR	CONC	Rigatona
-33.3	303.7	200	DOM	CONC	
-33.5	98.5	300	CAL	ASYM	Gefjun
-33.5	50.0	130	CAL	CONC	
-33.9	86.0	220	VOL	VOLC	Kunapipi
-34.5	288.0	200	DOM	R-CON	
-34.5	284.0	325 x 225	CIR	R-CON	
-34.7	266.3	180	CAL	CONC	
-35.0	135.0	2600	CAL	CONC	Artemis
-35.5	152.0	300	CIR	ASYM	
-36.0	298.5	375 x 330	CIR	ASYM	
-36.0	297.5	400	UNC		Tamiyo
-36.0	21.8	130	CIR		Pachamama
-36.3	6.0	400	CAL	CONC	Tamfana
-36.5	283.5	210	VOL	CONC	
-36.5	247.0	270 x 180	UNC	MULT	
-37.0	43.0	150	CAL	CONC	
-37.0	35.9	350 x 225	DOM	C-DR	Inanna
-37.0	293.0	375	CIR	ASYM	
-37.0	288.0	500	CAL	ASYM	
-37.5	70.5	200	CIR	C-DR	Indrani
-37.5	3.0	215	RAD	RAD	Carpo
-38.0	270.0	200 x 125	RAD	RAD	
-38.0	23.5	125	DOM	CONC	Ninhursag
-38.5	284.5	275	DOM	CONC	
-38.5	149.5	180	CAL	CONC	Teteoinnan
-38.6	291.2	200	CIR		Zywie
-38.6	287.0	225	RAD		Latta
-39.0	296.0	325	CIR	CONC	
-42.0	279.0	675	DOM	CONC	
-42.0	256.5	100	CAL	CONC	
-42.5	75.5	640 x 460	CIR	ASYM	Copia
-42.5	6.0	300	DOM	R-CON	Selu
-42.5	245.2	125	UNC	C-DR	
-45.0	287.5	225 x 150	DOM	MULT	
-45.5	55.5	225 x 175	CIR	R-CON	
-46.0	277.0	300	CAL	CONC	
-46.0	264.0	375 x 300	CAL	ASYM	
-46.5	80.0	200	CIR	CONC	Khotun
-46.8	258.2	175	UNC	CONC	
-46.8	20.2	200 x 110	CAL	C-CAL	Derceto
-47.0	85.0	275	CAL	C-DR	
-47.0	302.0	490	DOM	RAD	
-47.2	209.2	110	CAL	CONC	
-47.5	293.5	225	CAL	CONC	
-47.5	278.2	300	CAL		Ama
-48.0	88.3	125	CAL	CONC	Cailleach
-48.6	296.5	170	CAL		Navolga
-48.7	85.0	175	RAD	RAD	Makh
-49.0	59.5	175	DOM	CONC	
-50.0	289.5	225	CIR	CONC	
-51.5	289.5	110	CAL	CONC	
-52.3	14.6	170	CAL	C-CAL	Sarpanitum
-53.0	291.0	275	CAL	CONC	
-53.0	67.5	550	DOM		Marzyana
-53.5	95.5	350 x 275	CIR	ASYM	
-56.0	68.0	275	CAL	ASYM	
-57.0	30.0	455	CIR	C-DR	Otygen
-57.3	8.2	510	CIR	CONC	Eithinoha
-58.5	349.5	130	CAL	R-CON	Jord
-58.5	163.5	150	CAL	CONC	Fotla
-60.5	85.0	675	CAL	ASYM	
-62.0	241.0	150	CAL	CONC	
-63.5	322.5	300	RAD		Kamui Huci
-65.5	36.0	300	RAD	ASYM	
-66.0	84.0	330 x 225	CAL	MULT	
-66.5	209.5	100 x 75	CAL	ASYM	
-68.0	115.0	600	CAL	ASYM	
-67.0	0.0	800	CIR	ASYM	Quetzalpetlatl
-67.2	217.9	115	CAL		Ament
-69.3	66.0	415	CAL	CDR	
-73.0	97.0	200	CAL	CONC	
-77.5	30.0	525 x 225	CAL	ASYM	

Note. Class refers to classification given in the Stofan *et al.* (1992) data set. CONC, concentric; R-CON, radial concentric; C-CON, concentric caldera; C-DR, concentric-double ring; ASYM, asymmetric; MULT, multiple; RAD, radial; VOLC, volcanic (the latter two classes represent "Corona-like" features). Shape refers to the classification found in this study. CAL, calderic; CIR, circular; DOM, domal; UNC, uncertain; RAD, radial; VOLC, volcanic. Feature locations and diameters are taken from Stofan *et al.* (1992), Magee Roberts and Head (1993), and the USGS (1996) corona data sets.

9. APPENDIX: DISTRIBUTION OF CORONAE

Coronae were classified by normalizing the relief by the feature radius. Circular regions out to four corona radii were extracted from a 0.05° grid of Magellan altimetry records. North–south and east–west distances relative to the corona center were divided by the radius to give a normalized distance; normalized relief was found by dividing the relief relative to the lowest point in the region by corona radius.

The table includes 394 features, including 358 from the Stofan *et al.* (1992) data set, 27 additional features taken from the USGS-Flagstaff data base (1996), and 9 taken from Magee Roberts and Head (1993). Three corona shapes (domal, circular, and calderic) and two morphologies not related to coronae (radial and volcanic) are present. Variation between the corona shapes is gradational. The 54 domal coronae feature a central uplift with no surrounding moat; radial fracturing, if present, is typically visible only in the SAR images. The 93 circular coronae possess a flattened interior and an annular moat; in SAR images, these typically have concentric fractures and more well-defined lava flows. The 188 calderic coronae are those with more than 50% of the interior significantly lower than the surrounding plains; in SAR images, they are surrounded by degraded lava flows which are often indistinguishable from surrounding plains deposits.

Features distinctly differing from coronae include the 28 radial features, which posses a domal to flat topography, multiple calderas and evidence of lineament-related volcanism in scattered locations, and a further 9 volcanic features with broad, sloping flanks and evidence of extensive lava flows in SAR

images. A residual 22 features were unclassifiable, due to problems with the Magellan altimetry data set.

ACKNOWLEDGMENTS

This research was supported by NSF Grant EAR-9022476 and a NASA Grant from the Venus Data Analysis Program. In addition, we thank Maribeth H. Price and Daniel M. Janes for their reviews, and Roger Phillips and Noam Izenberg for their crater data set.

REFERENCES

Baer, G., G. Schubert, D. L. Bindschadler, and E. R. Stofan 1994. Spatial and temporal relations between coronae and extensional belts, northern Lada Terra, Venus. *J. Geophys. Res.* **99**, 8355–8369.

Basilevsky, A. T. 1998. Trends of tectonic evolution of Venus as deduced from stratigraphic studies and geologic mapping, *EOS, Transactions of the American Geophysical Union* (Spring Suppl.) **79**, S196.

Crumpler, L. S., J. W. Head, and J. C. Aubele 1993. Relation of major volcanic center concentrations on Venus to global tectonic patterns. *Science* **261**, 591–595.

Cyr, K. E., and H. J. Melosh 1993. Tectonic patterns and regional stresses near venusian coronae. *Icarus* **102**, 175–184.

DeLaughter, J. E., and D. M. Jurdy 1997. Venus resurfacing by coronae: Implications from impact craters. *Geophys. Res. Lett.* **24**, 815–818.

Grosfils, E. B., and J. W. Head 1994. The global distribution of giant radiating dike swarms on Venus: Implications for the global stress state. *Geophys. Res. Lett.* **21**, 701–704.

Grosfils, E. B., and J. W. Head 1996. The timing of giant radiating dike swarm emplacements on Venus: Implications for resurfacing of the planet and its subsequent evolution. *J. Geophys. Res.* **101**, 4645–4656.

Harder, H., and U. R. Christensen 1996. A one-plume model of martian mantle convection. *Nature* **380**, 507–509.

Hauck, S. A., R. J. Phillips, and M. H. Price 1997. Venus craters and resurfacing: More realistic constraints and models. In *Geodynamics of Venus: Evolution and Current State* (S. J. Mackwell and R. J. Phillips, Eds.), p. 8. [abstract]

Head, J. W., L. S. Crumpler, J. C. Aubele, J. E. Guest, and R. S. Saunders 1992. Venus volcanism: Classification of volcanic features and structures, associations, and global distribution from Magellan data. *J. Geophys. Res.* **97**, 13,153–13,197.

Herrick, R. R. 1994. Resurfacing history of Venus. *Geology* **22**, 703–706.

Ivanov, M. A., and J. W. Head 1998. Global stratigraphic units and major issues in Venus geology: Results from a geotraverse around Venus at 30 N latitude, *EOS, Transactions of the American Geophysical Union* (Spring Suppl.) **79**, S196.

Janes, D. M., S. W. Squyres, D. L. Bindschadler, G. Baer, G. Schubert, V. L. Sharpton, and E. R. Stofan 1992. Geophysical models for the formation and evolution of coronae on Venus. *J. Geophys. Res.* **97**, 16,055–16,067.

Jurdy, D. M., and M. J. Stefanick 1999. Correlation of Venus surface features, and geoid. *Icarus* **139**, 93–99.

Koch, D. M. 1994. A spreading drop model for plumes on Venus, *J. Geophys. Res.* **99**, 2035–2052.

Koch, D. M., and M. Manga 1996. Neutrally buoyant diapirs: A model for Venus coronae. *Geophys. Res. Lett.* **23**, 225–228.

Lancaster, M. G., J. E. Guest, and K. P. Magee 1995. Great lava flow fields on Venus. *Icarus* **118**, 69–86.

Magee Roberts, K., and J. W. Head 1993. Large-scale volcanism associated with coronae on Venus: Implications for formation and evolution. *Geophys. Res. Lett.* **20**, 1111–1114.

Manga, M., H. A. Stone, and R. J. O'Connell 1993. The interaction of plume heads with compositional discontinuities in the Earth's mantle. *J. Geophys. Res.* **98**, 19,979–19,990.

Nagasawa, C., M. Koyama, and S. Sasaki 1997. Change of stress field in Beta-Atla-Themis regio, estimated from surface geometry of dike swarms, stratigraphy of lavas and crater density. In *Geodynamics of Venus: Evolution and Current State* (S. J. Mackwell and R. J. Phillips, Eds.), p. 10. [abstract]

Namiki, N., and S. C. Solomon 1994. Impact crater densities on volcanoes and coronae on Venus: Implications for volcanic resurfacing. *Science* **265**, 929–933.

Phillips, R. J., R. E. Arvidson, J. M. Boyce, D. B. Campbell, J. E. Guest, G. G. Schaber, and L. A. Soderblom 1991. Impact craters on Venus: Initial analysis from Magellan. *Science* **252**, 288–297.

Phillips, R. J., and M. C. Malin 1983. The interior of Venus and tectonic implications. In *Venus* (D. M. Hunten, L. Colin, T. M. Donahue, and V. I. Moroz, Eds.), pp. 159–214, AGU Chapman Conference volume. Univ. Arizona Press, Tucson.

Phillips, R. J., R. F. Raubertas, R. E. Arvidson, I. C. Sarkar, R. R. Herrick, N. Izenberg, and R. E. Grimm 1992. Impact craters and Venus resurfacing history. *J. Geophys. Res.* **97**, 15,923–15,948.

Price, M. H. 1997. Free at last: A perspective on the CSR constraint. In *Geodynamics of Venus: Evolution and Current State* (S. J. Mackwell and R. J. Phillips, Eds.), p. 7. [abstract]

Price, M. H., G. Watson, J. Suppe, and C. Brankman 1996. Dating volcanism and rifting on Venus using impact crater densities. *J. Geophys. Res.* **101**, 4657–4671.

Schaber, G. G., R. G. Strom, H. J. Moore, L. A. Soderblom, R. L. Kirk, D. J. Chadwick, D. D. Dawson, L. R. Gaddis, J. M. Boyce, and J. Russell 1992. Geology and distribution of impact craters on Venus: What are they telling us? *J. Geophys. Res.* **97**, 13,257–13,301.

Squyres, S. W., D. M. Janes, G. Baer, D. L. Bindschadler, G. Schubert, V. L. Sharpton, and E. R. Stofan 1992. The morphology and evolution of coronae on Venus. *J. Geophys. Res.* **97**, 13,611–13,634.

Squyres, S. W., D. M. Janes, G. Schubert, D. L. Bindschadler, J. E. Moersch, D. L. Turcotte, and E. R. Stofan 1993. The spatial distribution of coronae and related features on Venus. *Geophys. Res. Lett.* **20**, 2965–2968.

Stefanick, M., and D. M. Jurdy 1996. Venus coronae, craters and chasmata. *J. Geophys. Res.* **101**, 4637–4643.

Stofan, E. R., and J. W. Head 1990. Coronae of Mnemosyne Regio: Morphology and origin. *Icarus* **83**, 216–243.

Stofan, E. R., V. L. Sharpton, G. Schubert, G. Baer, D. L. Bindschadler, D. M. Janes, and S. W. Squyres 1992. Global distribution and characteristics of coronae and related features on Venus: Implications for origin and relation to mantle processes. *J. Geophys. Res.* **97**, 13,347–13,378.

Strom, R. G., G. G. Schaber, and D. D. Dawson 1994. The global resurfacing of Venus. *J. Geophys. Res.* **99**, 10,899–10,926.

Watters, T. R., and D. M. Janes 1995. Coronae on Venus and Mars: Implications for similar structures on Earth, *Geology* **23**, 200–204.

Willis, J. J., and V. L. Hansen 1995. Caldera-related volcanism and collapse at Ishtar Terra, Venus. *Eos* **76**, F341. [abstract]